The Globular Cluster System of the Auriga Simulations

Timo L. R. Halbesma[1]⋆, Robert J. J. Grand[1], Volker Springel[1], Facundo A. Gómez[2,3], Federico Marinacci[4,5], Rüdiger Pakmor[1], Wilma Trick[1], Philipp Busch[1], Simon D. M. White[1]

[1] *Max-Planck-Institut für Astrophysik, Postfach 1317, D-85741 Garching, Germany*
[2] *Instituto de Investigación Multidisciplinar en Ciencia yTecnología, Universidad de La Serena, Raúl Bitrán 1305, La Serena, Chile*
[3] *Departamento de Física y Astronomía, Universidad de La Serena, Av. Juan Cisternas 1200 N, La Serena, Chile*
[4] *Department of Physics, Kavli Institute for Astrophysics and Space Research, MIT, Cambridge, MA 02139, USA*
[5] *Harvard-Smithsonian Center for Astrophysics, 60 Garden Street, Cambridge, MA 02138, USA*

ABSTRACT

> Ask SW whether I should ask Carlos Frenk and Adrian Jenkins for co-authorship

We investigate whether the galaxy formation model used for the Auriga simulations can produce a realistic globular cluster population at redshift zero. We compare properties of the simulated star particles in the Auriga haloes with catalogues of observations of the Milky Way globular cluster population available in the literature. We find that the Auriga simulations produce sufficient mass at radii and metallicities that are typical for the MW GCS, although we observe a varying mass-excess for the different R_{GC}-[Fe/H] bins. This implies different values for the combined product of the bound cluster formation efficiency and the globular cluster disruption rate. We investigate wether these differences could result from formation insitu vs. accreted star particles. We find ...

Key words: methods: numerical – galaxies: formation – galaxies: star clusters: general.

1 INTRODUCTION

> Paragraph: General introduction of GCs

• Diemand et al. (2005): "The radial profile of the stellar halo and metal-poor globular clusters of the Milky Way suggest that these components formed in rare early peaks above 2.5σ at redshift above 10. "

• Renaud et al. (2017): "GCs among oldest astrophysical objects. GCs form in the early Universe in highest density peaks (e.g. Diemand et al. 2005; Boley et al. 2009)"

• "Hence, they witness most of the formation and evolution processes of galaxies, and can be used to probe them" (Brodie & Strader 2006)

> Paragraph: scientific context / state of the field: briefly summarise previous work and references work of other groups

• Origin of the Milky Way globular clusters (Renaud et al. 2017)
• GCs in FIRE (Kim et al. 2018)
• EMOSAICS project (Pfeffer et al. 2018)
• GC-DMhalo connection (Boylan-Kolchin 2017)
• Origin of GC bimodality? (Fernandez & Bryan 2018)
• *GAIA* DR2: GC kinematics (Gaia Collaboration et al. 2018)
• Dating GC Tidal Disruption (Bose et al. 2018)
• GC in N-body simulation (Carlberg 2018)
• (Role of GC mass evolution on stream properties (Balbinot & Gieles 2018))
• GC formation from dwarfs to giants (Choksi et al. 2018)
• (GC contribution to EOR (Boylan-Kolchin 2018))
• Early Universe supermassive star / GC formation (Gieles et al. 2018)
• GC formation in cold filaments (Mandelker et al. 2018)
• GC formation in high-redshift dwarf galaxies (Zick et al. 2018)
• GCs in MW outer region (Peebles 2017)

⋆ E-mail: Halbesma@MPA-Garching.MPG.DE

• Impact of the Cutoff of the Cluster Initial Mass Function (Choksi & Gnedin 2018)

• Metallicity gradients in the globular cluster systems of early-type galaxies: in situ and accreted components (Forbes & Remus 2018)

• Globular clusters in M31, Local Group, and external galaxies (Larsen 2016)

• Globular Clusters Formed within Dark Halos I: present-day abundance, distribution and kinematics (Creasey et al. 2019)

• (The mass of the Milky Way from satellite dynamics (Callingham et al. 2018))

• Globular cluster formation and evolution in the context of cosmological galaxy assembly: open questions (Forbes et al. 2018)

• The kinematics of globular clusters systems in the outer halos of the Aquarius simulations (Veljanoski & Helmi 2016)

• Star Cluster Formation in Cosmological Simulations (Li et al. 2017, 2018; Li & Gnedin 2018)

• (A systematic analysis of star cluster disruption by tidal shocks - I. Controlled N-body simulations and a new theoretical model (Webb et al. 2018))

• Spatial mixing of binary stars in multiple-population globular clusters (Hong et al. 2018)

• Star Clusters Across Cosmic Time (Krumholz et al. 2018)

• Kinematics of Subclusters in Star Cluster Complexes: Imprint of their Parental Molecular Clouds (Fujii 2018)

• Investigating the population of Galactic star formation regions and star clusters within a Wide-Fast-Deep Coverage of the Galactic Plane (Prisinzano et al. 2018)

• Globular cluster number density profiles using *Gaia* DR2 (de Boer et al. 2019)

• Clustering Clusters: unsupervised learning on GC observations (of $\log M$, $\log \sigma_0$, $\log R_e$, [Fe/H], $\log |Z|$) to determine number of groups $k = 2$ (disk/halo) or $k = 3$ (disk/inner-halo/outer-halo): the optimal number of groups given the data is $k = 3$. (Pasquato & Chung 2019).

• There is a well-known hypothesis that Open Stars Clusters (OSCs) could form as a result of GCs crossing the disk. New kinematical data does not support this claim for two particular OSC-GC pairs, and does seem consistent with this scenario for six OSC-GC pairs (Bobylev & Bajkova 2019). (Note that GC crossing the disk could also trigger formation of multiple OSCs!)

• DM halo mass can be inferred from number of globular cluster in galaxy (Burkert & Forbes 2019)

• GCs in M31 outer halo (Wang et al. 2019)

> Paragraph, narrowing open questions in GC research down to formation, possibly "Bimodality suggests two formation mechanisms". In-situ formation vs. accretion in hierarchical build-up of galaxies naturally produces two populations of globular cluster.

• "colour bimodality, blue and red clusters (e.g. Zinn 1985; Gebhardt & Kissler-Patig 1999; Larsen et al. 2001; Peng et al. 2006)

• "blue metal-poor (with distribution peaking at [Fe/H] ≈ -1.5 for the Milky Way), no sign of rotation as a population (..) more metal-rich (peak at [Fe/H] ≈ -0.5 in the Milky Way) more spatially concentrated and rotating with the galaxy." (Harris 1996)

• "Blue clusters from in early Universe in galaxies that merge later. In (wet) merger process starbursts generate red population Ashman & Zepf (1992); Schweizer (1987)"

• "Forbes et al. (1997) propose instead that blue globulars form when the protogalaxy itself collapses, in a metal-poor and turbulence media. The red population would form later, once the galactic disc has settled. The formation of globular clusters would then be a multiphase process, with the first phase being interrupted possibly by cosmic reionization (Beasley et al. 2002)."

• "Kravtsov & Gnedin (2005); Li & Gnedin (2014) advocate that major mergers are at the origin of both subpopulations: blue clusters form during early mergers (z > 4) while the red ones appear in mergers at lower redshifts (even after z = 1). Although, this scenario, combined with star formation enhancement in mergers, seems appropriate in dense galactic environment leading to the assembly of massive elliptical galaxies, like in the Virgo Cluster as tested by Li & Gnedin (2014), it does not apply to Milky Way- like systems where no recent major merger took place (Wyse 2001; Deason et al. 2013; Ruchti et al. 2014, 2015).

• "Côté et al. (1998) argue that red clusters form in situ while the blue ones are accreted, either via merging satellite galaxies, or by tidal capture of the clusters themselves (see also Tonini 2013)."

> Paragraph: narrow the scientific motivation down to the scope of this particular work

• The star formation model implemented in the Auriga simulations is capable of producing a suite/population of realistic Milky Way-like galaxies at redshift zero.

• (However) State of the art simulations still face numerical restrictions that requires a subgrid approach to star formation and feedback because individual stars (and their evolution) cannot yet be accounted for. Star formation thus occurs in a heuristic/probabilistic fashion for gas cells that fulfill some star formation criterion. The star particles enrich the gas with metals and energy, both according to pre-defined/pre-calculated yields for specific feedback processes (supernova type I and II, strong stellar winds of asymptotic giant branch stars,). In addition, black holes are seeded in eligible haloes to account for feedback associated with an active galactic nucleus.

• The end-result of the star formation model is the production of simulated Milky Way-like galaxies. Therefore the question naturally arises whether or not the Auriga simulations are also capable of faithfully producing a globular cluster population as observed in the Milky Way.

• Globular cluster formation in cosmological zoom simulations is very interesting for two reasons. First of all, extragalactic observations typically show the integrated properties of globular clusters rather than that of the individual stars within the clusters. Moreover, the typical mass scale of globular clusters is comparable to the numerical (mass) resolution of cosmological zoom simulations. The detailed small scale physics that is at play for real world globular clusters appears in observations as the combined effect of the 10^{3-6} M$_\odot$, compared to a mass resolution of 10^{3-5} M$_\odot$ for the Auriga simulations. Globular clusters can therefore serve as

an ultimate test to the star formation model that is implemented in the numerical simulations. Secondly, cosmological zoom simulations provide an accurate recording of the full and detailed merger history of the simulated galaxy. This is important because theoretical paradigms for globular cluster formation in the literature know two distinct classes of GCs that are separated by their exact formation sites: an in-situ versus an accreted population. Cosmological zoom simulations uniquely allow for an investigation into globular cluster formation with particular focus on the in-situ and accreted populations.

Paragraph: Paper outline

We summarise the relevant characteristics of the Auriga simulations in section 2, followed by a summary of the observations of the Milky Way (MW) globular cluster system (GCS) in section 3 that we use to compare our simulations to in section 4. We discuss our findings in section 5 to come to our conclusions in section 6.

2 THE AURIGA SIMULATIONS

We use the Auriga simulations (Grand et al. 2017, hereafter G17), a suite of high-resolution cosmological zoom simulations of Milky Way-mass selected initial conditions. The simulations are performed with the state-of-the art code AREPO (Springel 2010; Pakmor et al. 2016), that solves the magnetohydrodynamical equations on a moving mesh, and an elaborate galaxy formation model that produces realistic spiral galaxies at redshift $z = 0$.

The interstellar medium is modelled using a sub-grid approach which implements the physical processes most relevant to galaxy formation and evolution. This model was tailored to the AREPO code and calibrated to reproduce key observables of galaxies, such as the history of the cosmic star formation rate density, the stellar mass to halo mass relation, and galaxy luminosity functions.

The sub-grid includes primordial and metal-line cooling with self-shielding corrections. Reionization is completed at redshift six by a time-varying spatially uniform UV background (Faucher-Giguère et al. 2009; Vogelsberger et al. 2013) The interstellar medium is described by an equation of state for a two-phase medium in pressure equilibrium (Springel & Hernquist 2003) with stochastic star formation in thermally unstable gas with a density threshold of $n = 0.13 \text{cm}^{-3}$, and consecutive stellar evolution is accounted for. Stars provide feedback by stellar winds (Marinacci et al. 2014; Grand et al. 2017), and further enrich the ISM with metals from SNIa, SNII, and AGB stars (Vogelsberger et al. 2013). The formation of black holes is modelled which results in feedback from active galactic nuclei (Springel et al. 2005; Marinacci et al. 2014; Grand et al. 2017). Finally, the simulations follow the evolution of a magnetic field of 10^{-14} (comoving) G seeded at $z = 127$ (Pakmor & Springel 2013; Pakmor et al. 2014). See G17 for further details of the numerical setup as well as the galaxy formation model.

TODO: paraphrase "The diversity in morphological properties of these simulated galaxies reflects the stochasticity inherent to the process of galaxy formation and evolution (e.g. Bullock & Johnston 2005; Cooper et al. 2010; Tumlinson 2010)."

Paragraph about Auriga's stellar haloes. "The Auriga Stellar Haloes: Connecting stellar population properties with accretion and merging history" Monachesi et al. (2018)

3 RELEVANT OBSERVATIONAL DATA

We summarise relevant observations of the globular cluster system of the Milky Way in Sec. 3.1, and of Andromeda (M31) in Sec. 3.2. In the remainder of the paper we compare observed (integrated) globular cluster properties to the Auriga simulations.

3.1 Milky Way

Harris (1996, 2010 edition; hereafter H96e10) provides a catalogue of the Milky Way globular cluster system that contains properties of 157 GCs. The authors initially estimated the size of the MW GCS to be 180 ± 10, thus, their catalogue to be ~85% complete. However, an additional 59 GCs have since been discovered by various authors. The total confirmed number of GCs in the MW adds up to 216 with new estimates now anticipating an additional thirty GCs yet to be discovered (e.g. Ryu & Lee 2018, and references therein).

Bica et al. (2019) communicate the latest efforts to aggregate the available data, presented in their CatClu catalog. Amongst 10978 star clusters and alike objects in the Milky Way, the catalog contains 200 GCs and 94 GC candidates. Unfortunately a machine readable version of the catalog is unavailable at this point in time. Therefore we utilise the H96e10 dataset nonetheless, but we caution that the Harris catalogue is now believed to be (only) 53-72% complete.

The relevant data fields that we use from H96e10 are the metallicity [Fe/H], the Galactic distance components X, Y, and Z (in kpc)[1], and absolute magnitude in the V-band M_V. We use the latter to calculate mass-estimates by assuming $M_{V,\odot} = 4.83$ and a mass to light ratio $M/L_V = 1.7 \text{ M}/\text{L}_\odot$, the mean for MW clusters (McLaughlin & van der Marel 2005).

Age estimates

We supplement H96e10 with age-estimates from isochrone fits to stars near the main-sequence turnoff in 55 GCs (VandenBerg et al. 2013, hereafter V13). The mean value of the age-estimates in this data set is 11.9 ± 0.1 Gyr and the dispersion is 0.9 Gyr. Furthermore, only one of the 55 GC age-estimates is below 10 Gyr.

---

[1] In a Sun-centered coordinate system: X points toward Galactic center, Y in direction of Galactic rotation, and Z toward the North Galactic Pole. We calculate the galactocentric radius $R_{\text{GC}} = \sqrt{(X - R_\odot)^2 + Y^2 + Z^2}$, assuming the solar radius $R_\odot = 8$ kpc.
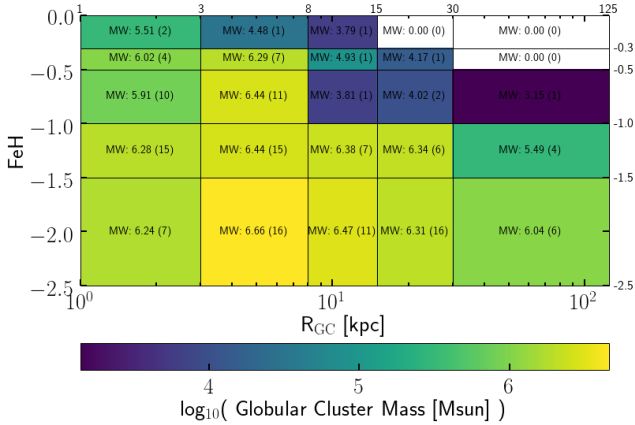
Figure 1. Mass-weighted r_{gc}-[Fe/H] distribution of 151 GCs in the MW (data from Harris 1996, 2010 ed.), which is 98.19 % of the total MW GCS mass in the Harris catalog.

Distribution of total GC mass in metallicity-radial bins

In Fig. 1 we show the two-dimensional mass-weighted metallicity-radial distribution of the MW GCS. In Sec. 4.3 we investigate whether the star formation model implemented in the Auriga simulations can produce sufficient total mass in GC candidates in the same bins.

3.2 Andromeda

The fifth revision of the revised bologna catalogue (RBC 5, last updated August, 2012) is the latest edition of three decades of systematically collecting integrated properties of the globular cluster system of the Andromeda galaxy (Galleti et al. 2004, and references therein). One contribution to RBC 5 is the work by Caldwell et al. (2011, hereafter C11). C11 delivers a uniform set of spectroscopic observations 316 out of the 339 GCs in the inner $1°.6 (\sim 21)$ kpc, calibrated using the Milky Way GCS.

Globular clusters in the outer halo of M31, up to projected radii $R_{\mathrm{proj}} \sim 150$ kpc, are observed in the Pan-Andromeda Archaeological Survey (PAndAS, Huxor et al. 2014, hereafter H14), see also Veljanoski et al. (2014); Mackey et al. (2019). H14 presents the discovery of 59 new GCs and publishes updates to RBC 5. The work of H14 is incorporated in the latest version[2] of the C11 dataset. It seems that the 2015 edition of C11 is the most recent aggregated dataset M31's GCS and we will therefore use this troughout the remainder of this work.

The relevant fields in the C11 dataset are the age, metallicities, and absolute visual magnitude.

> TODO: paraphrase "For M31 GC masses we combine the catalogues of Caldwell et al. (2011, using the given masses) and Huxor et al. (2014, again assuming $M/L_V = 1.7$ M$_\odot$, e.g. Strader, Caldwell & Seth 2011)."

For M31 we find an age distribution with a mean value of 10.8±10.8 Gyr and a dispersion of 2.3 Gyr. Furthermore,

---

[2] dated 23 Sep 2015; retrieved from https://www.cfa.harvard.edu/oir/eg/m31clusters/M31_Hectospec.html
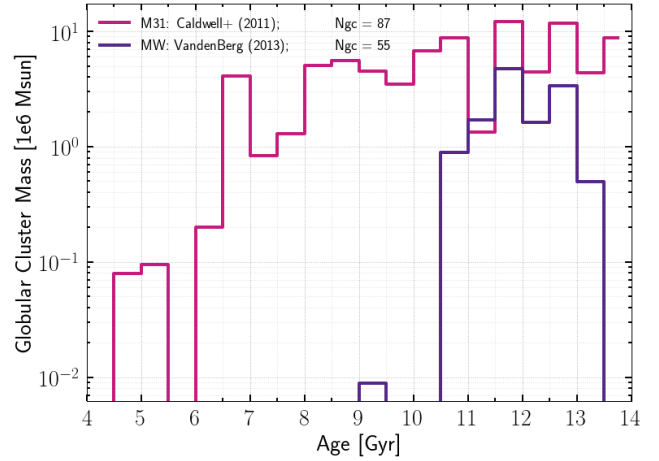

Figure 2. Mass-weighted age distribution of 55 GCs in the MW (data from VandenBerg et al. 2013) and 87 GCs in M31 (data from Caldwell et al. 2011).

27 GCs have age-estimates below 10 Gyr, and the minimum age is 4.8 Gyr.

$$\tag{1}$$

where (α_1, δ_1) are the right ascension and declination (in degrees, We adopt the values $(\alpha_1, \delta_1) = (0^{\mathrm{h}}42^{\mathrm{m}}44.3^{\mathrm{s}}, +41°16'9")$ (TODO: reference), and $D_{\mathrm{M31}} = 778$ kpc (TODO: reference).

4   RESULTS

We define GC candidates in the Auriga simulations as all star particles older than 10 Gyr. The mean age-estimate of the 55 MW GCs in V13 is 11.9 ± 0.1 Gyr with a dispersion of 0.8 Gyr, and the age-estimate for only one observed GC is smaller than 10 Gyr.

Through out the analysis we use six sub sets of star particles: *all stars*, and *old stars* (age > 10 Gyr, GC candidates hereafter). Both sub sets are further split up in (old) star particles that have formed *in-situ* (bound to the most-massive halo/subhalo in the first snapshot that the star particle was recorded), and (old) *accreted* star particles (i.e. those that have formed ex-situ and are bound to the most-massive halo/subhalo at $z = 0$).

In Sec. 4.1 we investigate the metallicity distribution of the GC candidates, in Sec. 4.2 we show the distribution of galactocentric radii of the globular cluster candidates within the Auriga simulations, and we combine both in Sec. 4.3. We continue our analysis with an investigation of the properties of the proto-galaxies at times of birth of the accreted globular cluster population in Sec. 4.6

4.1   Metallicity distribution

We investigate whether the star formation model implemented in the Auriga simulations is capable of producing sufficient mass in old star particles in each metallicity bin in comparison to the Milky Way and Andromeda globular
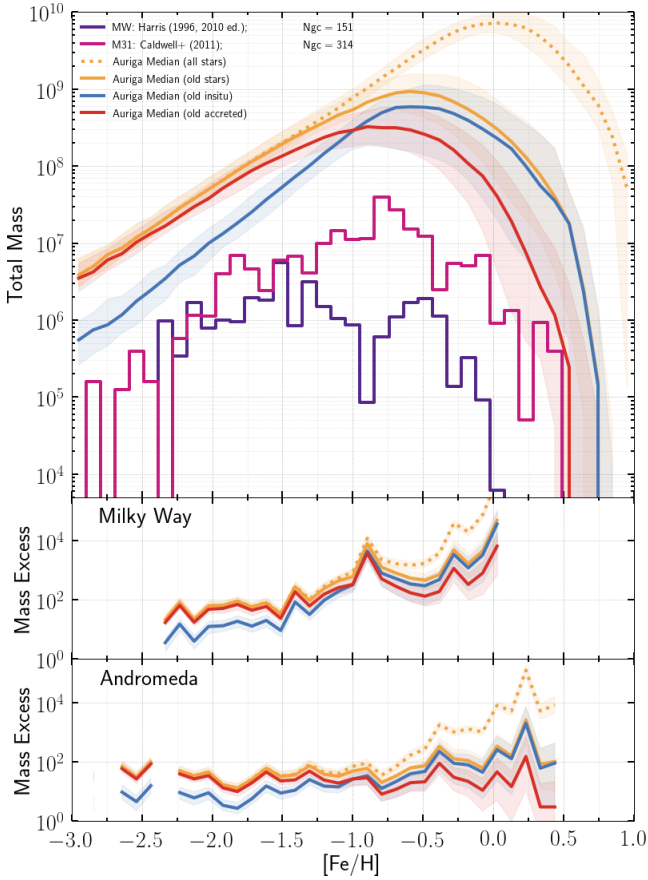
Figure 3. Mass-weighted metallicity distribution of star particles in the Auriga simulations. We show the median value of all Auriga haloes for all stars (orange dotted) and globular cluster candidates (i.e. stars with age > 10 Gyr; orange solid). The latter sub set is further split up between stars that formed in-situ (blue solid), and those that were accreted (red solid). Shaded regions indicate the 1σ interval. The MW (M31) GCS is shown in purple (magenta). The middle (bottom) panel shows the ratio of the simulated mass to the mass in the MW (M31) GCS.

cluster systems. In Fig. 3 we show a mass-weighted metallicity distribution where the lines show the median value of all thirty Auriga level 4 haloes for *all stars* (orange dotted), *old stars / GC candidates* (orange solid), *old in-situ* stars (blue solid), and *old accreted* stars (red solid). The shaded regions indicate the 1σ interval around the median (i.e. the scatter between runs with different initial conditions and merger histories). The MW (M31) GCS is shown in purple (magenta). We use the same bin sizes for the simulations as for the observations, explicitly shown for the observed profiles.

The peak of the distribution shifts down from [Fe/H] ∼ 0.0 to ∼ −0.6 for the *old stars* compared to *all stars* while the mass at the peak lowers by roughly one dex. Moreover, we find that the metallicity range −3 < [Fe/H] < −1 is only populated by the GC candidates, while [Fe/H] > −1 is dominated by star particles younger than 10 Gyr. Furthermore, the *old accreted* sub set contributes most significantly to the range −3 < [Fe/H] < −1, and the contribution of the *old in-situ* stars at these metallicities declines steeper with declining metallicity than the *old accreted* population. We

note that the scatter between different Auriga haloes is much smaller than the difference between the MW and M31 GCSs. We conclude that old star particles in the Auriga simulation suite as a whole cannot be consistent with both the Milky Way and the Andromeda globular cluster system.

The middle (bottom) panel shows the ratio of the simulated mass to the mass in the MW (M31) GCS. We observe an increasing trend with increasing metallicity for the Milky Way over the entire range of the data, while the M31 GCS shows this increase only in the range [Fe/H]>-0.5 (although not for the *old accreted* component.

Furthermore we test the null hypothesis that the metallicity distribution of the MW (M31) GCS and the *old*, *old insitu*, and *old accreted* star particles in the Auriga simulations are drawn from the same underlying distribution. We calculate the two-sample Kolmogorov-Smirnov test statistic for all thirty Auriga level 4 haloes and reject the null hypothesis for every halo, for every sub set of star particles at least at the 99.99% confidence level. In addition, the null hypothesis that the metallicity distributions of the MW and M31 GCS are drawn from the same distribution is rejected at the 99.99997% confidence level.

4.2 Radial distribution

Somewhat arbitrarily, I will take the region $r_p > 3$ kpc (containing 75 clusters) as the fiducial Mikly Way sample. If we were to view the Mikly Way at the same inclination angle to the disk as we see M31, this cutoff in projected distance would correspond roughly to the inner distance limits in the M31 halo sample.

Is the spatial distribution of the GC candidates in the Auriga simulations consistent with the MW GCS?

> Look into Pandromeda survey. Star counts, very wide angle survey

4.3 Metallicity-radial distribution

What age-metallicity distribution is produced by star formation events in the Auriga simulations? ?

4.4 Metallicity-radial distribution: higher resolution

> Do we even want this?

4.5 From star particles to globular clusters

Star particles are not globular clusters. Many stars do form in clusters, but not all clusters end up gravitationally bound. Star particles in the Auriga simulations represent single-age stellar populations that have formed at the same location within the galaxy. Therefore one could assume a model for the star cluster formation efficiency Γ, which could be used to 'convert' star particles to bound star clusters e.g. Kruijssen (2012). This model relies on the local birth properties of the star particles. However, in our analysis we can retrieve the properties of the star particle in the first snapshot it was
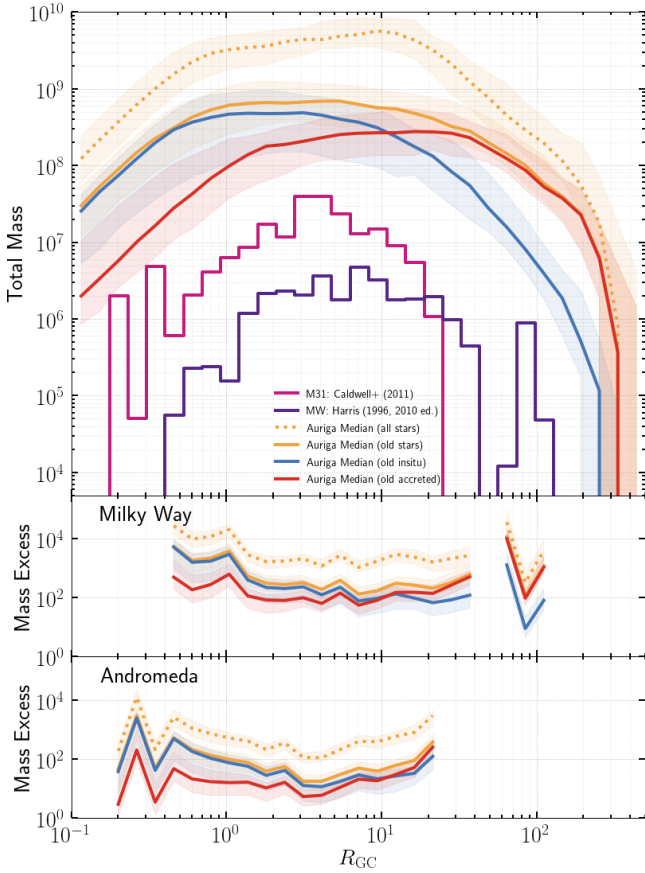
Figure 4. Mass-weighted distribution of (two-dimensional) galactocentric radii at which star particles in the Auriga simulations are found. For Andromeda we show the projected galactocentric radius, assuming its center is located at $(0^h42^m44.3^s, +41°16'9")$ at a distance of 778 kpc.

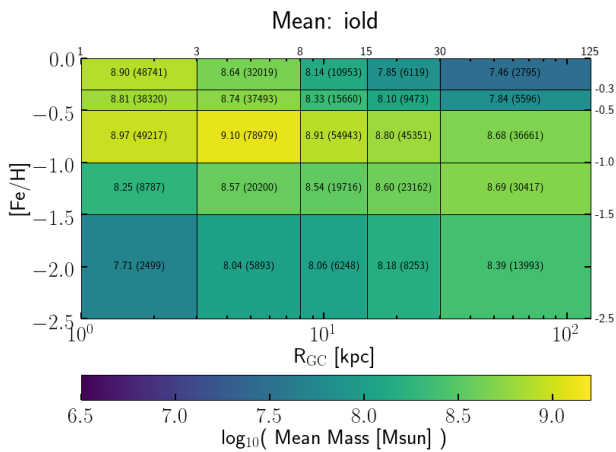**Figure 5.** Mass-weighted [Fe/H]-R_{GC} distribution of all Auriga haloes (level 3, 4 and 5). Here we consider the old (> 10 Gyr) stars in all simulations and color-code the **mean value** (of 40 Auriga haloes)
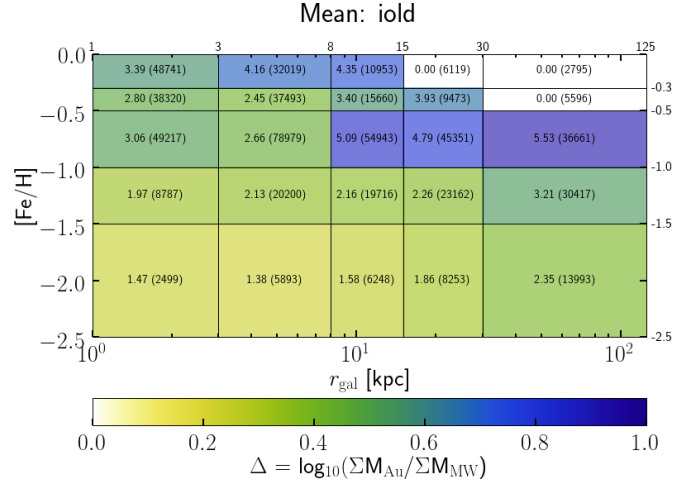

Figure 6. Ratio
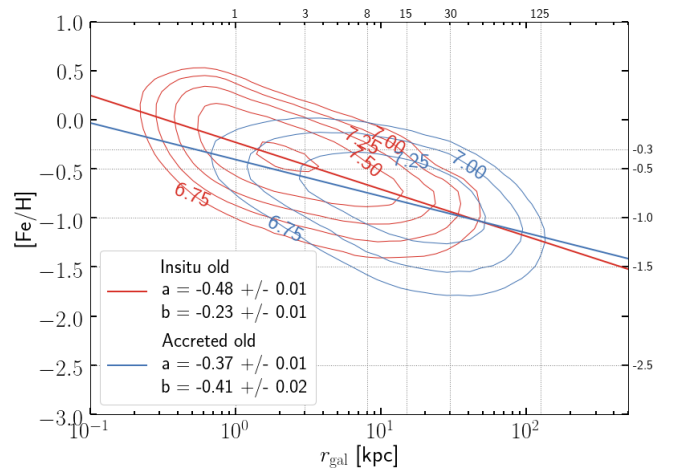
Figure 7. TODO: add 1σ interval around both relations, and flip x and y.

recorded, but not the gas properties at times of birth. Therefore we are unable to model the formation of star clusters in more detail.

Furthermore, we compare star particles to present-day globular clusters, thereby ignoring the effects of (dynamical) disruption of globular clusters over nearly a Hubble time. As shown by Pfeffer et al. (2018), a detailed model of the tidal history of star clusters requires a temporal resolution of order mega year. For the Auriga level 4 simulations we have 128 snapshots for the age of the Universe, thus, a far too coarse temporal resolution for meaningful calculations.

Therefore we investigate the over-production of simulated mass in the metallicity and radial bins and use the term 'efficiency' to refer to the combined product of bound cluster formation and globular cluster disruption. In Fig. **??** we show the efficiencies that we find when we compare the simulations to the globular cluster systems of the Milky Way as well as that of Andromeda (M31).

4.6 Properties of birth haloes of the accreted population

Auriga galaxy /w 5 Myr snapshots.

4.7 Age-metallicity distribution

What age-metallicity distribution is produced by star formation events in the Auriga simulations?

4.8 Formation history

Can we identify particular star formation events that generate GC candidates with the correct age, metallicity, and radial properties as expected or the MW GCS?

Can we distinguish between particles that have formed in-situ and those that have been accreted? Can we identify specific features in the age-metallicity plane, or in the $R_{\mathbf{GC}}$-[Fe/H] plane, that result from one of both populations? How does this connect to proposed mechanisms for globular cluster formation in the literature?

Orbits: are the pericentres different? Look at velocity + specific angular momentum distribution in the different FeH/Rgc bins as proxy for the pericenter

5 DISCUSSION

We investigate all star particles in the Auriga simulations that are older than 10 Gyr, an approach equal to the method of (Renaud et al. 2017). This approach does not take the bound cluster fraction (e.g. Kruijssen 2012) into account. This means that our sub set, which is based on selection by age, comprises both stars in the field as well as globular clusters. We compare the total mass in the simulations in metallicity ([Fe/H]), galactocentric radius R_{GC}, and [Fe/H]-R_{GC} bins to the total mass in the MW GCS (using the H96e10 data set). The mass excess in the simulations gives a maximum mass loss 'budget' for the product of cluster formation efficiency and dynamical evolution. We find fractions that vary with metallicity, radius and metallicity-and-radius.

> "The fraction of all star formation that occurs in bound stellar clusters (the cluster formation efficiency, hereafter CFE) follows by integration of these local clustering and survival properties over the full density spectrum of the ISM, and hence is set by galaxy-scale physics. We derive the CFE as a function of observable galaxy properties, and find that it increases with the gas surface density" (Kruijssen 2012)

5.1 Age cut

Although the age distribution of M31 Perhaps an age cut of 6 Gyr would would be more appropriate for M31, see Fig. 2.

6 SUMMARY AND CONCLUSIONS

Check Auriga boilerplate that we need to acknowledge

REFERENCES

Ashman K. M., Zepf S. E., 1992, ApJ, 384, 50
Balbinot E., Gieles M., 2018, MNRAS, 474, 2479
Beasley M. A., Baugh C. M., Forbes D. A., Sharples R. M., Frenk C. S., 2002, MNRAS, 333, 383
Bica E., Pavani D. B., Bonatto C. J., Lima E. F., 2019, AJ, 157, 12
Bobylev V. V., Bajkova A. T., 2019, arXiv e-prints, p. arXiv:1901.06481
Boley A. C., Lake G., Read J., Teyssier R., 2009, ApJ, 706, L192
Bose S., Ginsburg I., Loeb A., 2018, ApJ, 859, L13
Boylan-Kolchin M., 2017, MNRAS, 472, 3120
Boylan-Kolchin M., 2018, MNRAS, 479, 332
Brodie J. P., Strader J., 2006, ARA&A, 44, 193
Bullock J. S., Johnston K. V., 2005, ApJ, 635, 931
Burkert A., Forbes D., 2019, arXiv e-prints,
Caldwell N., Schiavon R., Morrison H., Rose J. A., Harding P., 2011, AJ, 141, 61
Callingham T., et al., 2018, arXiv e-prints,
Carlberg R. G., 2018, ApJ, 861, 69
Choksi N., Gnedin O. Y., 2018, arXiv e-prints,
Choksi N., Gnedin O. Y., Li H., 2018, MNRAS, 480, 2343
Cooper A. P., et al., 2010, MNRAS, 406, 744
Côté P., Marzke R. O., West M. J., 1998, ApJ, 501, 554
Creasey P., Sales L. V., Peng E. W., Sameie O., 2019, MNRAS, 482, 219
Diemand J., Madau P., Moore B., 2005, MNRAS, 364, 367
Faucher-Giguère C.-A., Lidz A., Zaldarriaga M., Hernquist L., 2009, ApJ, 703, 1416
Fernandez R., Bryan G. L., 2018, MNRAS, 479, 200
Forbes D. A., Remus R.-S., 2018, MNRAS, 479, 4760
Forbes D. A., Brodie J. P., Grillmair C. J., 1997, AJ, 113, 1652
Forbes D. A., et al., 2018, Proceedings of the Royal Society of London Series A, 474, 20170616
Fujii M. S., 2018, arXiv e-prints, p. arXiv:1812.01858
Gaia Collaboration et al., 2018, A&A, 616, A12
Galleti S., Federici L., Bellazzini M., Fusi Pecci F., Macrina S., 2004, A&A, 416, 917
Gebhardt K., Kissler-Patig M., 1999, AJ, 118, 1526
Gieles M., et al., 2018, MNRAS, 478, 2461
Grand R. J. J., et al., 2017, MNRAS, 467, 179
Harris W. E., 1996, AJ, 112, 1487
Hong J., Patel S., Vesperini E., Webb J. J., Dalessandro E., 2018, MNRAS, p. 3147
Huxor A. P., et al., 2014, MNRAS, 442, 2165
Kim J.-h., et al., 2018, MNRAS, 474, 4232
Kravtsov A. V., Gnedin O. Y., 2005, ApJ, 623, 650

Kruijssen J. M. D., 2012, MNRAS, 426, 3008

Krumholz M. R., McKee C. F., Bland-Hawthorn J., 2018, arXiv e-prints, p. arXiv:1812.01615

Larsen S. S., 2016, in Bragaglia A., Arnaboldi M., Rejkuba M., Romano D., eds, IAU Symposium Vol. 317, The General Assembly of Galaxy Halos: Structure, Origin and Evolution. pp 120–127, doi:10.1017/S1743921315006821

Larsen S. S., Brodie J. P., Huchra J. P., Forbes D. A., Grillmair C. J., 2001, AJ, 121, 2974

Li H., Gnedin O. Y., 2014, ApJ, 796, 10

Li H., Gnedin O. Y., 2018, preprint, (arXiv:1810.11036)

Li H., Gnedin O. Y., Gnedin N. Y., Meng X., Semenov V. A., Kravtsov A. V., 2017, ApJ, 834, 69

Li H., Gnedin O. Y., Gnedin N. Y., 2018, ApJ, 861, 107

Mackey A. D., et al., 2019, MNRAS, 484, 1756

Mandelker N., van Dokkum P. G., Brodie J. P., van den Bosch F. C., Ceverino D., 2018, ApJ, 861, 148

Marinacci F., Pakmor R., Springel V., 2014, MNRAS, 437, 1750

McLaughlin D. E., van der Marel R. P., 2005, ApJS, 161, 304

Monachesi A., et al., 2018, preprint, (arXiv:1804.07798)

Pakmor R., Springel V., 2013, MNRAS, 432, 176

Pakmor R., Marinacci F., Springel V., 2014, ApJ, 783, L20

Pakmor R., Springel V., Bauer A., Mocz P., Munoz D. J., Ohlmann S. T., Schaal K., Zhu C., 2016, MNRAS, 455, 1134

Pasquato M., Chung C., 2019, arXiv e-prints, p. arXiv:1901.05354

Peebles P. J. E., 2017, preprint, (arXiv:1708.04542)

Peng E. W., et al., 2006, ApJ, 639, 95

Pfeffer J., Kruijssen J. M. D., Crain R. A., Bastian N., 2018, MNRAS, 475, 4309

Prisinzano L., et al., 2018, arXiv e-prints, p. arXiv:1812.03025

Renaud F., Agertz O., Gieles M., 2017, MNRAS, 465, 3622

Ryu J., Lee M. G., 2018, ApJ, 863, L38

Schweizer F., 1987, in Faber S. M., ed., Nearly Normal Galaxies. From the Planck Time to the Present. pp 18–25

Springel V., 2010, MNRAS, 401, 791

Springel V., Hernquist L., 2003, MNRAS, 339, 289

Springel V., Di Matteo T., Hernquist L., 2005, MNRAS, 361, 776

Tonini C., 2013, ApJ, 762, 39

Tumlinson J., 2010, ApJ, 708, 1398

VandenBerg D. A., Brogaard K., Leaman R., Casagrande L., 2013, ApJ, 775, 134

Veljanoski J., Helmi A., 2016, A&A, 592, A55

Veljanoski J., et al., 2014, MNRAS, 442, 2929

Vogelsberger M., Genel S., Sijacki D., Torrey P., Springel V., Hernquist L., 2013, MNRAS, 436, 3031

Wang S., Ma J., Liu J., 2019, arXiv e-prints

Webb J. J., Reina-Campos M., Kruijssen J. M. D., 2018, arXiv e-prints, p. arXiv:1812.00014

Zick T. O., Weisz D. R., Boylan-Kolchin M., 2018, MNRAS, 477, 480

Zinn R., 1985, ApJ, 293, 424

de Boer T. J. L., Gieles M., Balbinot E., Henault-Brunet V., Sollima A., Watkins L. L., Claydon I., 2019, arXiv e-prints,

APPENDIX A: SCATTER BETWEEN INDIVIDUAL AURIGA HALOES, AND NUMERICAL CONVERGENCE

We check whether the properties of the Auriga globular cluster candidates are well converged between the three different resolution levels used for the Auriga simulations. Here we consider all three Auriga haloes for which simulation runs were performed at all three resolution levels: Au6, Au16, and Au24. Here we can investigate differences between individual haloes.

Fig. A1 shows the mass-weighted metallicity distribution, Fig. A2 shows the mass-weighted radial distribution, and Fig. **??**

This paper has been typeset from a TEX/LATEX file prepared by the author.
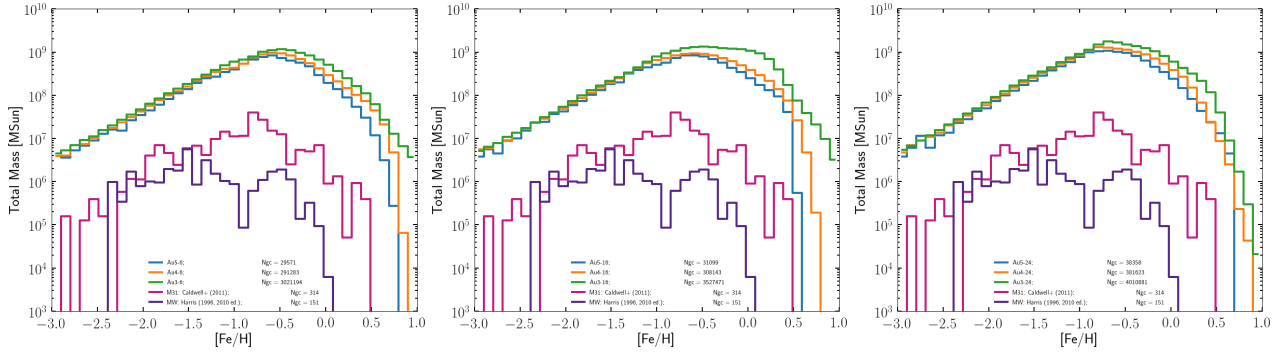
Figure A1. Same as Fig. 3, but here the colours indicate resolution level: L3 green, L4 orange, and L5 blue. *Left:* Auriga halo 6. *Mid:* Auriga halo 16. *Right:* Auriga halo 24. For all three haloes we find marginal increases in the mass normalization with increasing resolution level.
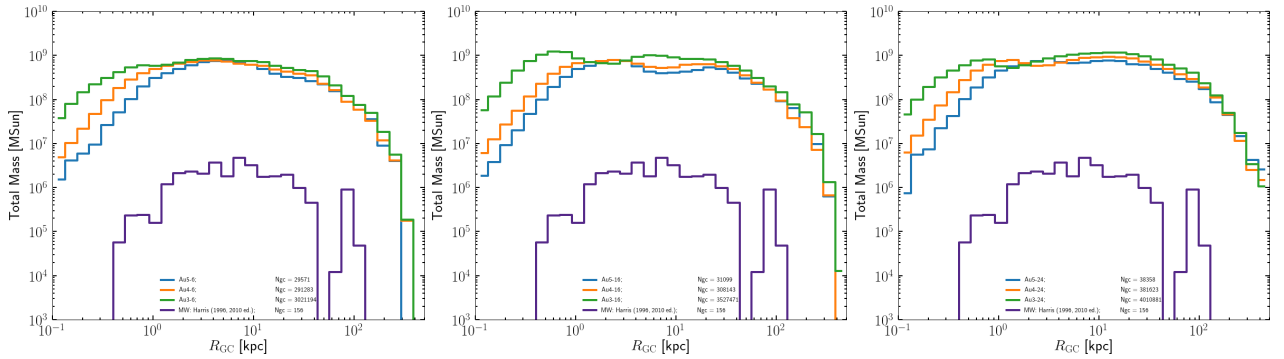

Figure A2. Same as Fig. 4, but here the colours indicate resolution level: L3 green, L4 orange, and L5 blue. *Left:* Auriga halo 6. *Mid:* Auriga halo 16. *Right:* Auriga halo 24. For all three haloes we find marginal increases in the mass normalization with increasing resolution level.